Research article

polymers advanced technologies

Received: 29 August 2015, Revised: 2 December 2015, Accepted: 19 December 2015, Published online in Wiley Online Library: 9 February 2016

(wileyonlinelibrary.com) DOI: 10.1002/pat.3753

Phase behavior and Li+ Ion conductivity of styrene-ethylene oxide multiblock copolymer electrolytes†

Joel M. Sarapas[a], Kenji Saijo[b], Yue Zhao[a,c], Mikihito Takenaka[b] and Gregory N. Tew[a]*

Solid polymer electrolytes are attractive materials for use as battery separators. Here, a molecular weight series of polystyrene–polyethylene oxide (PEO) multiblock copolymers was synthesized by the thiol–norbornene click reaction. The subsequent materials were characterized both neat and with a lithium *bis*-(trifluoromethane)sulfonimide salt loading [(Li)/(EO)] of 0.1. In general, neat samples demonstrated crystallinity scaling with PEO content. Lithium ion-containing samples had broad scattering peaks, half of which displayed disordered scattering, even at the lowest block molecular weights (polystyrene = 1 kg/mol, PEO = 1 kg/mol). Fitting of disordered scattering data, using the random phase approximation, yielded χ_{RPA} and R_g values that were compared with recent predictive work by Balsara and coworkers. The predictions were accurate near the volume fraction $f_{PEO} = 0.5$ but deviated symmetrically with volume fraction asymmetry. Samples were also analyzed by electrochemical impedance spectroscopy for their potential to conduct lithium ions. Samples with $f_{PEO} \geq 0.5$ demonstrated robust conductivity, whereas samples below this volume fraction conducted very poorly, with one exception ($f_{PEO} = 0.24$). This work expanded upon our recently reported approach to multiblock copolymer synthesis, demonstrating the improved access of materials to further our fundamental understanding of multiblock copolymers. Copyright © 2016 John Wiley & Sons, Ltd.
Supporting information may be found in the online version of this article.

Keywords: multi-block copolymer; polystyrene; ethylene oxide; ion conductivity; click

INTRODUCTION

Block copolymers represent a class of materials of long-standing interest to materials scientists, physicists, and chemists. One of their most noteworthy features, microphase separation, occurs when two (or more) covalently tethered and chemically distinct blocks become immiscible.[1–4] This material property has been exploited in many applications and remains an active area of research.[5–12] The point at which phase separation occurs, as well as the morphology generated, depends on the segregation strength between the separated blocks and the volume fraction (f) of the blocks.[13] Segregation strength, generally written as χN, is the product of the Flory–Huggins chemical mismatch parameter, χ, and the degree of polymerization, N. By changing these three variables (χ, N, f), many different morphologies can be accessed, including lamellar, hexagonal cylinders, spheres, and the bicontinuous gyroid phase.[1,14,15] These phases and the conditions under which they occur are well understood within the relatively simple diblock copolymer system. However, increasing the number of chemically distinct blocks by just one yields an entirely new family of hybrid morphologies, demonstrating the complexity of higher order block copolymers.[6] As a result, there has been an increased interest in materials with both more chemically distinct blocks, as well as with a greater number of blocks.[16] These materials, referred to as multiblock copolymers (MBCs), are themselves their own class of materials, with phase separation thermodynamics and kinetics distinct from, yet familiar to their diblock cousins.[17–19] The multiblock architecture has been shown to increase toughness of otherwise brittle materials as well as produce more disordered phase separation when compared with expected morphologies.[20–23] Both of these properties are advantageous for many applications, but the implementation of MBCs into common use has historically been hampered by their difficult synthesis, specifically sequential block addition by living polymerization.[16,24] Most prolifically, anionic polymerization has produced well-defined controlled MBCs that have played key roles in the fundamental understanding of MBC properties.[16,17] Reversible addition–fragmentation chain transfer has also recently been implemented to synthesize an undecablock copolymer with exquisite sequence control.[25] However, the sensitivity of both of these polymerizations to

* Correspondence to: Gregory N. Tew, Department of Polymer Science and Engineering, University of Massachusetts, Amherst, MA 01003 USA.
E-mail: tew@mail.pse.umass.edu

† Associated Content: DSC/WAXS data, GPC measurements, and RPA fitting details are provided in the supporting information.

a J. M. Sarapas, Y. Zhao, G. N. Tew
Department of Polymer Science and Engineering, University of Massachusetts, Amherst, MA, 01003, USA

b K. Saijo, M. Takenaka
Department of Polymer Chemistry; Graduate School of Engineering, Kyoto University, Nishikyo-ku, Kyoto, 615-8510, Japan

c Y. Zhao
Quantum Beam Science Center, Japan Atomic Energy Agency, Tokai, Ibaraki, 319-1195, Japan

ambient conditions, coupled with the requirement of numerous monomer additions, creates a need for simple, more tolerant MBC syntheses.

To achieve a more straightforward synthesis, as well as incorporate more varied monomer structures, techniques have been developed to synthesize MBCs with a polydisperse block number by connecting telechelic macromonomers together using high yielding reactions. Reports include urethane formation,[20,23] acid chloride condensation,[26] alkyne azide click chemistry,[27,28] and thiol–Michael addition.[29] Our group recently reported MBC synthesis utilizing thiol–ene click chemistry, by linking telechelic dithiol macromonomers with telechelic di-norbornene macromonomers.[30] This synthesis is air and water tolerant, and the resulting MBCs were thermally stable above 300 °C due to the nature of the thiol–ether linkage. Koo *et al.* reported low conversions associated with thiol–ene polymer–polymer conjugation, an issue that was largely avoided by using the thiol–norbornene addition.[31] This specific thiol–ene addition has been shown several times to be the most thermodynamically and kinetically favorable thiol–ene reaction.[32–34] In this study, we expand our library of MBCs prepared by thiol–norbornene chemistry to materials incorporating polystyrene (PS) and polyethylene oxide (PEO). PS and PEO were chosen specifically to be able to study these materials both neat, and as block copolymer electrolytes (BCEs) for lithium ion batteries. PS–PEO diblock copolymers are particularly well studied BCEs, extended here to MBCs for comparison.

Block copolymer electrolytes used for lithium ion batteries commonly contain two block chemistries with specific properties: one block capable of dissolving and shuttling lithium ions through the material, and one block that is mechanically rigid, providing support as well as inhibiting dendritic growth that would otherwise cause a short in the system.[35–41] This approach also eliminates toxic and flammable organic solvents commonly associated with traditional lithium batteries. PS–block–PEO electrolytes, a particularly popular BCE system dubbed "SEO", contain PEO for lithium solvation and conduction, and PS for mechanical stability and resistance to dendritic growth.[38,40,42,43] Work on optimizing conduction efficiency indicates that smaller grain size, or more poorly oriented lamellae, provides materials with conductivities five times greater than their ordered counterparts.[37,44] Because of reports of MBCs displaying disordered phase separation, styrene-ethylene oxide (SEO) MBC materials could indeed be strong candidates for lithium ion conduction. Materials developed to explore this hypothesis are depicted in Fig. 1. Samples are indexed by the molecular weight of their constituent macromonomers, with the first value within the brackets corresponding to the PS block molecular weight and the second value corresponding to the PEO block molecular weight, both in kg/mol. For example, sample **SEO[1-1]** is the MBC with **PEO 1** and **PS 1** as its constituent macromonomers. Samples that include the lithium salt lithium *bis*-(trifluoromethane)sulfonimide (LiTFSI) are indicated by the suffix –Li.

Recently, Teran *et al.* reported a rigorous study of SEO BCE thermodynamics.[45] A molecular weight series of nearly symmetric SEO block copolymers, between 3 and 15 kg/mol, were analyzed at varying salt concentrations and temperatures, using the random phase approximation (RPA) fit on disordered scattering to determine the effective Flory–Huggins parameter, χ_{eff}, for a given set of conditions.[46] The dependence of χ_{eff} for PS and PEO containing LiTFSI (PEO–Li) as a function of the degree of polymerization N, temperature T, and r [defined as (Li)/(EO)] was determined, and the following equation was reported:[45]

$$\chi_{eff} = A(T) + \frac{B(T)}{N} + \frac{C(T)}{N}\left[1 - \exp\left(\frac{-D(T)r}{N}\right)\right] \qquad (1)$$

where $A(T)$, $B(T)$, $C(T)$, and $D(T)$ are listed in the Supporting Information (SI).

We applied this model to our samples, recognizing that it was created using samples near symmetric volume fractions, and may not hold for highly asymmetric samples. Also, here, we look at MBC samples instead of diblock copolymers, further complicating this approximation. We also used the RPA fit for diblock copolymers to estimate an experimental, qualitative χ_{RPA} value for salt containing samples that display disordered scattering, and compared the two results.

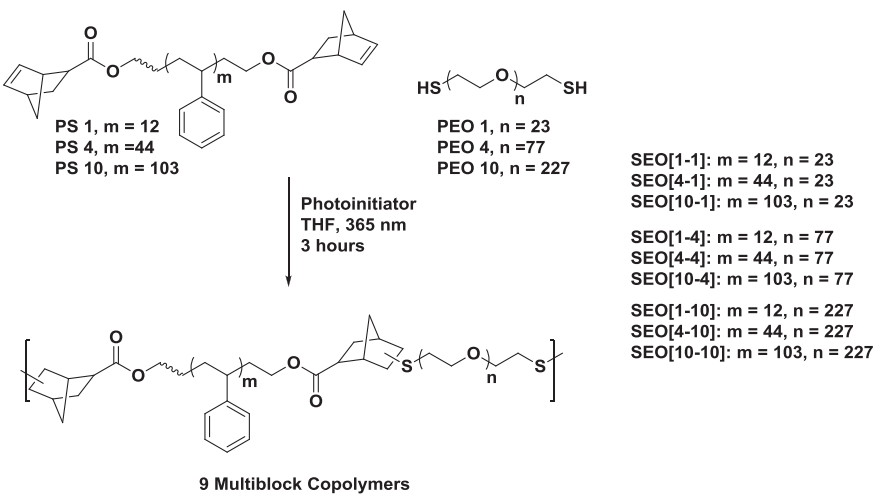

Figure 1. Synthesis of **SEO** multiblock copolymer molecular weight series. The wavy bond of polystyrene (PS) indicates synthesis from a bifunctional initiator. The two numbers inside the brackets correspond to the molecular weight, in kg/mol, of the corresponding PS and polyethylene oxide (PEO) macromonomers, respectively.

EXPERIMENTAL

Materials

Norbornene carboxylic acid (*exo*/*endo* mixture), triphenyl phosphine, diisopropyl azodicarboxylate, di-hydroxy terminated polystyrene, di-thiol PEO, and Irgacure 2959 were purchased from Sigma Aldrich, Alfa Aesar, Acros Organics, Laysan Bio, or Polymer Source and were used without further purification. The chemical structure of di-norbornene polystyrene is provided in Fig. S1.

Macromonomer/multiblock copolymer synthesis

Macromonomers and MBCs were synthesized according to our previous reports.[30,47] ^{1}H NMR of **PS 1** functionalized with norbornene is shown in Fig. S1. ^{1}H NMR spectra were recorded at 300 MHz using a Bruker DPX-300 NMR spectrometer. MBCs were synthesized by the thiol–norbornene click reaction. Stoichiometric amounts of PS and PEO macromonomers were dissolved in dry tetrahydrofuran (THF) at a concentration of 100 mg/mL, along with 2 wt% photoinitiator. Samples were exposed to ultraviolet light (365 nm) for 2 h, precipitated into pentane, and dried for 24 h at 85 °C. Molecular weights observed by gel permeation chromatography (GPC) are tabulated in Table S1.

Polymer electrolyte preparation

Polymer electrolytes were prepared by adding a solution of LiTFSI in dry THF to neat MBC samples. Upon complete solvation, samples were dried under vacuum at 110 °C for 24 h. Samples were used as is for differential scanning calorimetry (DSC), small-angle X-ray scattering (SAXS), and electrochemical impedance spectroscopy (EIS).

Gel permeation chromatography

Both macromonomers and MBCs were analyzed by GPC. Average block number was calculated using the result of the corresponding macromonomer molecular weights based on PS standards. Molecular weight values of macromonomers used to calculate number of blocks and MBC molecular weights are tabulated in Table S1. GPC was performed using Agilent 1260 series system with a PL gel 5 μm guard column, two 5 μm analytical Mixed C columns, and a 5 μm analytical Mixed D column (Agilent), incubated to 40 °C. THF was used as the eluent at a flow rate of 1.0 mL/min. PS standards were used for the calibration, and toluene was used for the flow marker.

Differential scanning calorimetry

Samples with and without salt were measured into TA aluminum DSC pans and hermetically sealed. Sample masses varied from 3 to 5 mg. Pans were run vs an empty standard pan on a TA Q200, following a heat-cool-heat procedure. Samples were heated to 150 °C at 10 °C/min, cooled to −80 °C at 5 °C/min and re-heated to 150 °C. Presented data are the final heating curve. Final heating curves of samples with **PEO 1** and **PEO 10** macromonomers are displayed in Fig. S2. Percent crystallinity is reported in Fig. S5.

X-Ray scattering

Neat MBC samples were annealed at 130 °C for 3 h and cooled to room temperature before scattering measurements were performed. Scattering of neat samples was performed using the Kyoto University SAXS apparatus (NANO-Viewer IP system, Rigaku Co. Ltd. Japan). The instrument consists of 1.2 kW (40 kV, 30 mA) rotating-anode X-ray generator (RA-Micro 7HF) with multilayer optics (Conforcal Max-Flux optics) for focusing and monochromatizing ($\lambda = 0.154$ nm; the wavelength of X-ray), a 2270 mm camera (1000 mm from the source to the sample and 1270 mm from the sample to the detector) including three pinhole slits (0.4, 0.2 and 0.45 mm$^{\varphi}$ from upper stream) between the source and the sample, and two-dimensional (2D) imaging plate detector (R-AXIS IV++). Wide-angle X-ray scattering (WAXS) measurements were carried out with the same X-ray optics used for the SAXS measurements except for reducing the sample-to-detector distance into 130 mm. Exposure time for taking an X-ray scattering pattern was 3600 s. The obtained 2D data were corrected for the absorption of the sample, subtracted air and background scattering, and converted to one-dimensional data by circularly averaging.

Salt containing samples for SAXS were prepared as described. SAXS patterns were obtained from an Osmic MaxFlux Cu Kα X-ray source with a wavelength of 1.54 Å and a 2D gas-filled wire array detector (both Molecular Metrology, Inc.) at a distance of 1.476 m from the sample. The raw data were calibrated against the peak position of a silver behenate standard which has a scattering vector of $q = 1.076$ L/nm. 2D images were reduced to the one-dimensional form using angular integration. Domain spacings were calculated from the principal scattering maxima (q*) calculated using $d = 2\pi/q^*$.

Transmission electron microscopy

Samples were annealed at 130 °C for 3 h, cooled to room temperature, and sectioned, producing 50–100 nm films using a Leica Ultracut at −80 °C. The films were stained under saturated RuO_4 vapor, and imaged using a JEM 2000FX at 200 kV.

Electrochemical impedance spectroscopy

Scanning electron microscope aluminum mounts were coated with gold using a Cressington 108 sputter coater. Teflon disks with a small hole ($d = 0.03$ cm) were fixed to the mounts, and a concentrated (200 mg/mL) solution of MBC/electrolyte in THF was cast into the hole. Samples were dried under nitrogen, and then loaded into a custom apparatus described in a previous report.[48] Samples were held at 125 °C for 4 h to remove residual solvent and ambient moisture then cooled to room temperature. Impedence spectra from 10 MHz to 0.1 Hz were taken every 30 min during cooling. Sample **SEO[4-4]-Li** is omitted from our data set.

χN and volume fraction predictions

Values of χ were predicted with an equation developed by Balsara and coworkers, used in their work predominantly for symmetric or near symmetric PS–PEO diblock copolymers, and thus includes a correction factor to account for the presence of LiTFSI salt at varying concentrations.[45] The χ values of the MBCs, both with and without salt, were determined by treating each sample as although it were a diblock of the two constituent macromonomers, a calculation necessary due to the *N* dependence of the prediction. PEO volume fractions, f_{PEO}, were calculated according to the literature.[43]

RESULTS AND DISCUSSION

di-Hydroxy-polystyrene functionalization

The functionalization of each dihydroxy-PS macromonomer with two norbornene units was assessed by ^{1}H NMR. Macromonomers **PS 1** and **PS 4** demonstrated near quantitative norbornene addition based on the ratio of aromatic pendant-group protons to the double-bond protons of norbornene that appear at 6.0 ppm (Fig. S1).[47,48] The aromatic styryl peaks overlap with the solvent signal, but solvent contribution to the overall peak integration was nearly negligible due to the concentration of the samples. The norbornene double-bond peaks in macromonomer **PS 10** were too dilute, due to the increased molecular weight, to quantify the degree of norbornene functionalization, but their presence and the macromonomers' subsequent reactivity confirms at least partial norbornene functionalization.

Multiblock copolymer synthesis

After exposure to ultraviolet light, all nine MBC thiol–ene click reactions became significantly more viscous, indicating an increase in molecular weight and MBC formation. Comparing GPC traces of crude MBC reactions with their corresponding macromonomers revealed MBC peaks corresponding to molecular weights several times those of their constituent macromonomers. A representative overlay can be found in Fig. 2. The MBC GPC traces were multimodal, indicating not only that several block lengths of multiblocks existed but often the unreacted macromonomer was also present. The average number of blocks per MBC, ‹*n*›, is reported in Table 1, while detailed molecular weight characterization is cataloged in Tables S1 and S2. While some values of ‹*n*› seem small, it is important to note that ‹*n*› is decreased by residual macromonomer or low block count MBCs because the entire molecular weight range was integrated, but for many of the MBC samples, the principal peak by GPC has a much higher number of blocks than the overall trace. For example, integrating the entire GPC trace for **SEO[1-1]** yields ‹*n*› = 6, but integrating the principle peak alone yields an ‹n^*› of 11. After precipitation and drying, the samples appeared homogeneous and did not exhibit homopolymer-multiblock macrophase separation, where homopolymer is unreacted macromonomer. Thus, after precipitation, the samples were used and analyzed as is, because the approach here is to generate and study easily synthesized materials.

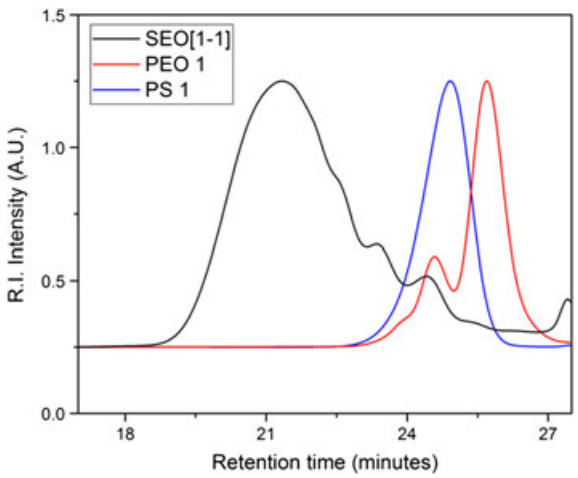

Figure 2. Representative normalized gel permeation chromatography traces of **SEO[1-1]** (black line, post precipitation) and its corresponding macromonomers **PEO 1** (red line), and **PS 1** (blue line). Higher molecular weight peaks associated with **PEO 1** are likely disulfide linkages. Traces were obtained in THF at a flow rate of 1 mL/min and analyzed with respect to polystyrene standards. This figure is available in colour online at wileyonlinelibrary.com/journal/pat

Generally, reactions that involved smaller molecular weight constituent macromonomers yielded MBCs with a higher number of blocks than those that utilized higher molecular weight macromonomers. Notably, MBCs that contained macromonomer **PEO 10** were limited in their average number of blocks. This could be a function of the decreased chain end concentration, which ultimately decreases the number of collisions and thus extent of reaction observed with this macromonomer. However, because a less significant drop in ‹*n*› was seen when using **PS 10**, it is possible that **PEO 10** simply has a lower degree of thiol functionalization than its lower molecular weight counterparts. Another possibility is that the molecular weight estimation of macromonomer **PEO 10** was not correct, which would affect the stoichiometry of the thiol–ene click reaction and ultimately suppress chain extension in this condensation polymerization-style process. No effort was made here to improve the conversion of the reactions involving **PEO 10**.

The dispersity of the resulting MBCs varied from 1.3 to 2.1, significantly higher than their counterpart macromonomers, which were purchased commercially and made via controlled polymerization processes. A broad MBC distribution is indicative of a broad range of multiblock species within a single sample, a characteristic of step-growth MBCs.

Thermal properties and crystallinity

Differential scanning calorimetry was employed to observe T_g behavior, as well as to determine the extent of PEO crystallinity within MBC samples in both the presence and absence of salt (full data set in Table S3). WAXS measurements were used to supplement crystallinity information in samples without salt (**SEO[1-4]**, **SEO[4-4]**, **SEO[10-4]**, and **SEO[10-4]-Li** in Fig. 3, remainder in the SI). **SEO[1-1]**, **SEO[4-1]**, and **SEO[10-1]**, containing macromonomer **PEO 1**, exhibited no melting endotherm by DSC and only amorphous scattering by WAXS (Figs S2 and S3). This finding is unsurprising, as low molecular weight PEO blocks in block copolymers, even at appreciable volume fractions, have difficulty crystallizing. The salt free MBCs also displayed a faint T_g associated with PEO near −35 °C, an increased value that can be attributed to partial mixing with the PS phase.[49] **SEO[4-1]** and **SEO[10-1]** also had PS T_g values at 58 and 83 °C, respectively, corresponding to the **PS 4** and **PS 10** macromonomers used. Both T_g depressions demonstrate partial mixing of PEO into the PS phase, a phenomenon that is more pronounced in **SEO[4-1]** than **SEO[10-1]**, due to the lower molecular weight PS component and thus increased ease of mixing. **SEO[1-1]** did not have a detectable PS T_g, although the DSC curve exhibited a permanent slope change near 0 °C (Fig. S2).

Multiblock copolymers using the intermediate molecular weight macromonomer **PEO 4**, **SEO[1-4]**, **SEO[4-4]**, and **SEO [10-4]**, demonstrated a much wider variety of thermal and crystalline properties, displayed in Fig. 3. **SEO[1-4]**, were found to be highly crystalline with a sharp melting endotherm at 46 °C and sharp, well-pronounced peaks via WAXS corresponding to the

Table 1. Molecular weight data for SEO multiblock copolymers

Sample	PS macromonomer	PEO Macromonomer	f_{PEO}[a]	$\langle n \rangle$[b]	$\langle n^* \rangle$[c]
SEO[1-1]	PS 1	PEO 1	0.41	6	11
SEO[4-1]	PS 4	PEO 1	0.16	6	12
SEO[10-1]	PS 10	PEO 1	0.08	5	7
SEO[1-4]	PS 1	PEO 4	0.70	3	7
SEO[4-4]	PS 4	PEO 4	0.40	6	9
SEO[10-4]	PS 10	PEO 4	0.22	5	7
SEO[1-10]	PS 1	PEO 10	0.87	2	3
SEO[4-10]	PS 4	PEO 10	0.66	3	4
SEO[10-10]	PS 10	PEO 10	0.45	2	4

PEO, polyethylene oxide; PS, polystyrene.
[a]Volume fraction of polyethylene oxide without salt, calculated by the densities and starting masses of each macromonomer.
[b]Average number of macromonomer blocks in each MBC calculated by GPC of macromonomers and final sample using M_n values.
[c]Average block number of principal peak, calculated using M_p values.

PEO crystal lattice. Additionally, due to the small size of the PS component, strong mixing into the PEO phase was also observed in the form of an increased PEO T_g at −16 °C. PEO crystallinity was significantly suppressed in **SEO[4-4]**, with the melting endotherm decreasing from 82.0 for **SEO[1-4]** to 6.4 J/g, while the WAXS pattern was dominated by amorphous scattering, with only slight peaks indicating minor crystallinity. The melting temperature was also slightly decreased to 41 °C. Based on the crystallinity of **SEO[1-4]**, it is clear that MBCs containing **PEO 4** are capable of crystallizing, and that the sharp melting endotherm decrease in **SEO[4-4]** can be explained by increasing PS content to the point where PEO chains can no longer rearrange to crystallize. This effect was further amplified in the case of **SEO[10-4]**, which used the highest PS molecular weight macromonomer, and was completely void of crystallinity, both via DSC and WAXS. More subtle mixing of PS into the PEO phase was also observed with **SEO[4-4]** and **SEO[10-4]**, which have PEO T_g values of around −37 °C.

The **PEO 10** series, **SEO[1-10]**, **SEO[4-10]**, and **SEO[10-10]**, all had melting endotherms, as well as prominent scattering peaks in their WAXS patterns (Figs S2 and S3). The melting endotherms observed in DSC decreased as PS content increased, from 119.2 for **SEO[1-10]** to 78.2 J/g for **SEO[4-10]**, and finally 53.3 J/g for **SEO[10-10]**. This can be explained by the increase in PS per mass with these samples, and thus, the ratio of available crystalline polymer was decreased. Percent crystallinity is plotted as a function of volume fraction in the SI to support this argument (Fig. S5). WAXS patterns followed a similar trend, where while PEO crystallinity seemed to decrease as PS volume fraction increased, amorphous scattering from PS also began to contribute more and covered shorter peaks closer to the baseline.

The addition of LiTFSI, with an *r* ratio of 0.1, eradicated crystallinity in all nine MBCs as measured by DSC (**SEO[1-10]** in Fig. 3**,** remaining in Fig. S2). This is a common observation as LiTFSI is known to readily dissolve in PEO, leading to the disruption of the EO crystal lattice.[50] An increase in the PS T_g was also observed for **SEO[4-1**] and **SEO[10-1]** upon salt addition, by 21 and 3 °C, respectively. These increases are indicative of demixing between the PEO-Li and PS phases. This can be explained by the increase in the χ value achieved upon dissolving ions in the EO phase. This proved useful, as it allowed us to study SEO MBCs with and without crystals at room temperature and varying χ parameters.

Morphological characterization

Phase separation and morphology were assessed by SAXS for all MBCs, both with and without salt. MBCs without salt and a majority PEO composition (**SEO[1-4]**, **SEO[1-10]**, **SEO[4-10]**, and **SEO[10-10]**) displayed patterns consistent with crystalline lamellae, although the resulting peaks were noticeably broader than those observed for neat PEO. Mixing of PS in amorphous PEO may be a contributor to this peak broadening. Heating these samples above their melting temperature (80 °C) eradicated scattering peaks for **SEO[1-4]**, **SEO[1-10]**, and **SEO[4-10]**, demonstrating that phase separation within these three samples is driven exclusively by crystallinity at room temperature. MBCs synthesized with macromonomer **PEO 10** (**SEO[1-10]**, **SEO[4-10]**, and **SEO[10-10]**) are displayed in Fig. 4, both at room temperature and 80 °C. **SEO[10-10]** retained its principle peak at 80 °C, likely due to the symmetric nature of this multiblock, as well as its higher *N* compared with the other MBCs. The domain spacing observed for **SEO[10-10]** at 80 °C was similar to that obtained at room temperature, indicating that while crystallinity exists at room temperature, these crystals likely exist within a morphology dictated by phase separation achieved during annealing. This conclusion is supported by a room temperature transmission electron micrograph (TEM) of **SEO[10-10]** (Fig. 5), which shows poorly ordered lamellae domains of a similar length scale (20 nm) as obtained by SAXS at both temperatures.

The addition of LiTFSI salt to the MBCs dramatically changed the scattering patterns of all nine MBCs (Fig. 6). As discussed earlier, the addition of LiTFSI at $r = 0.1$ is sufficient to eliminate room temperature crystallinity from all MBC samples, and thus scattering associated with PEO crystallinity. Additionally, the solvation of LiTFSI in PEO increases the χ value, leading to a new PS–PEO_{salt} interaction parameter, χ_{eff}. Because of the increased interaction parameter, **SEO[1-1]-Li**, **SEO[4-1]-Li**, and **SEO[10-1]-Li** developed patterns with broad peaks that shifted to lower *q* values as the styrene block length increased. These samples are particularly notable as they displayed no scattering in their no-salt state. Two other samples, **SEO[1-4]-Li** and **SEO[1-10]-Li**, also

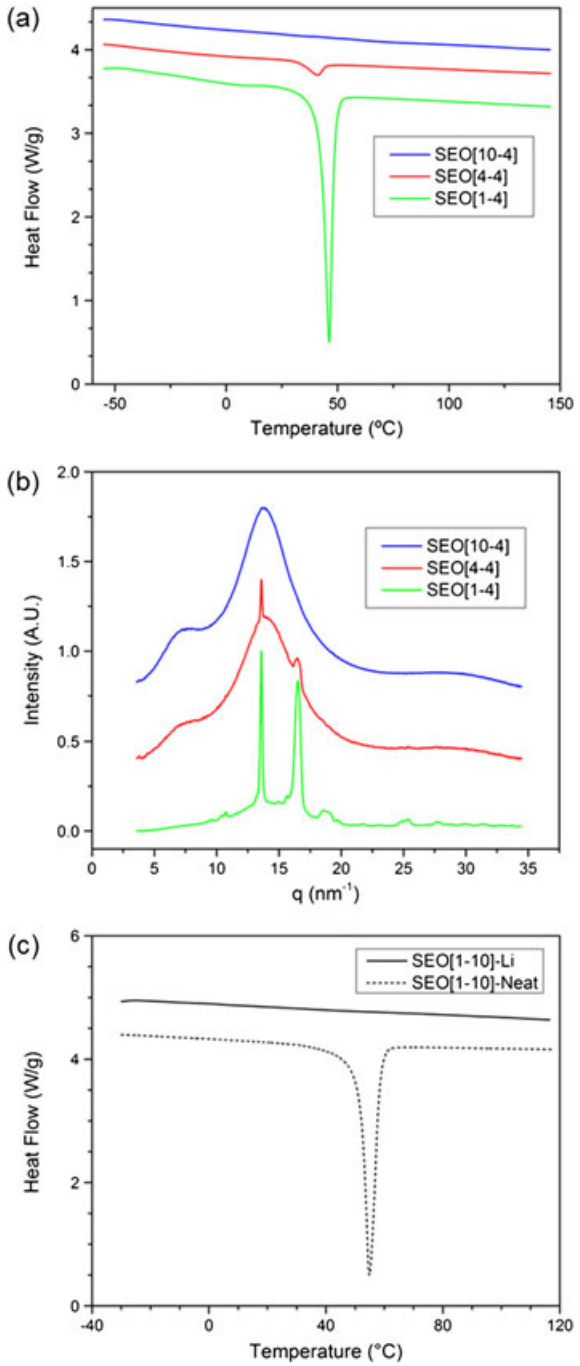

Figure 3. Differential scanning calorimetry of (a) **SEO[1-4]** (green line), **SEO[4-4]** (red line), and **SEO[10-4]** (blue line) and (b) WAXS patterns of **SEO[1-4]** (green line), **SEO[4-4]** (red line), and **SEO[10-4]** (blue line). (c) Differential scanning calorimetry of **SEO[1-10]** (black line) and **SEO[1-10]-Li** (dashed line). This figure is available in colour online at wileyonlinelibrary.com/journal/pat

displayed disordered scattering, a sharp contrast from **SEO[1-4]** to **SEO[1-10]**, which were completely dominated by crystallinity at room temperature and displayed no phase separation at 80 °C.

Samples **SEO[10-4]-Li** and **SEO[4-10]-Li**, with more intermediate volume fractions compared with samples displaying disordered scattering, had SAXS patterns with two peaks, q^* and $2q^*$. Because of the lack of higher order peaks, however, we refrain from making any exact morphological assignment, although

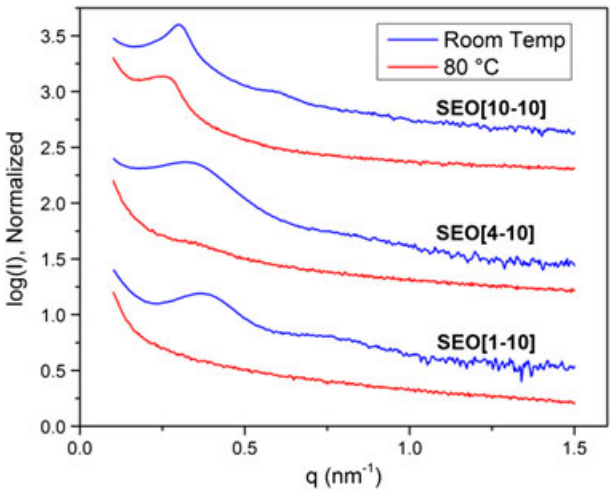

Figure 4. Small-angle X-ray scattering patterns of **SEO[10-10]** (top), **SEO[4-10]** (middle), and **SEO[1-10]** (bottom) at room temperature (blue) and 80 °C (red). Data are shifted for clarity. This figure is available in colour online at wileyonlinelibrary.com/journal/pat

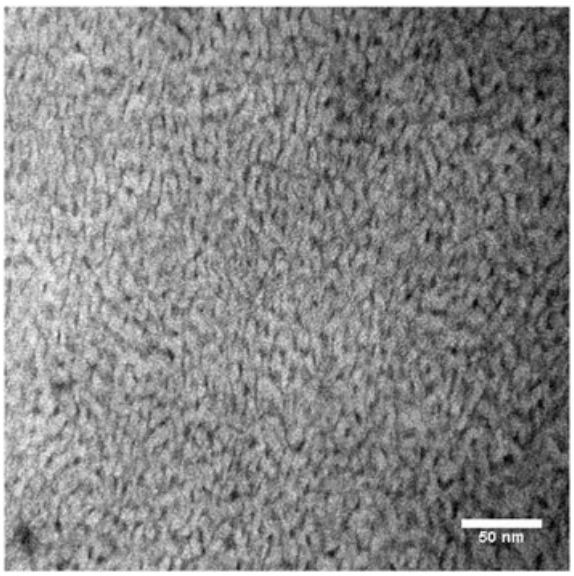

Figure 5. Transmission electron micrograph of **SEO[10-10]** at 250 k magnification.

both samples are in the volume fraction region common for cylinders or lamellae. Regardless, the broad nature of the peaks indicates poorly aligned or poorly ordered phases. **SEO[10-10]-Li** was more easily interpreted, with clearer peaks developing at q^* and $3q^*$, a common pattern seen in symmetric lamellar samples. The width of the peaks in **SEO[10-10]-Li** contrasts with the broad peaks in **SEO[10-4]-Li** and **SEO[4-10]-Li**, demonstrating a relatively more ordered morphology, with grains of about 300 nm as determined by the Scherrer equation.[44,51]

Fitting of disordered scattering

Samples that displayed disordered scattering with salt, **SEO[1-1]-Li**, **SEO[4-1]-Li**, **SEO[1-4]-Li**, **SEO[10-1]-Li**, and **SEO[1-10]-Li**, were fit using the RPA, elucidating values of χ (noted as χ_{RPA}) and R_g. Because of the presence of many different species of

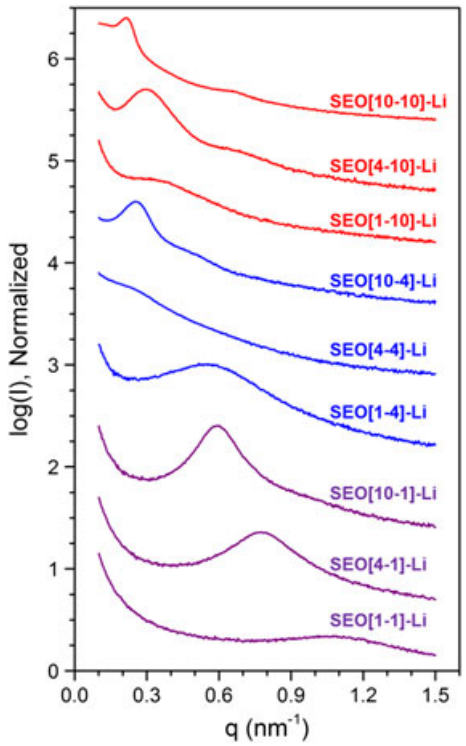

Figure 6. Room temperature normalized SAXS patterns of all multiblock copolymers at a lithium *bis*-(trifluoromethane)sulfonimide salt loading of $r = 0.1$. Samples are color-coded by polyethylene oxide (PEO) macromonomer, **PEO 1** (purple curves), **PEO 4** (blue curves), and **PEO 10** (red curves). This figure is available in colour online at wileyonlinelibrary.com/journal/pat

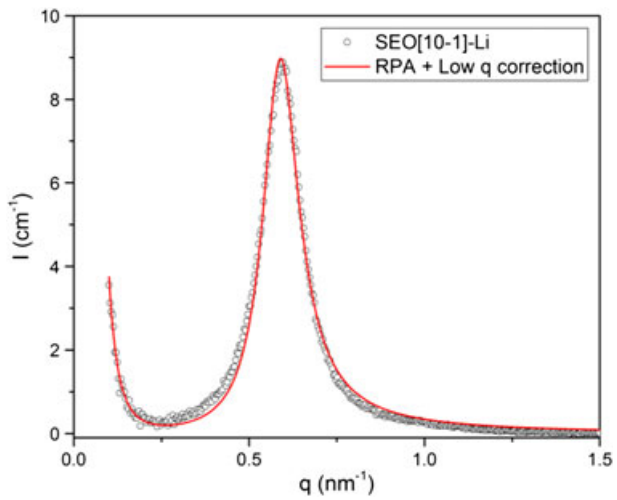

Figure 7. Representative random phase approximation (RPA) fit of the **SEO**[10-1] scattering pattern. Low-q interference was removed for the initial fitting and added here to the fit to match the original data. This figure is available in colour online at wileyonlinelibrary.com/journal/pat

block lengths, all samples were approximated as diblock copolymers with N values corresponding to the sum of repeat units for the corresponding macromonomer pairs. For example, the N value used for **SEO[1-1]** is the sum of N for **PEO 1** and **PS 1**. Thus, χ_{RPA} and R_g should be regarded as qualitative. A representative fit is displayed in Fig. 7 for **SEO[10-1]-Li** (consult the SI for fitting details). The resulting χ_{RPA} from our sample values were compared to those calculated using eqn 1, χ_{eff}. A summary of χ values and their percent differences as well as R_g values determined by the RPA fit are shown in Table 2. Values of R_g seemed to scale strongly with the degree of polymerization of the diblock unit, with the lowest R_g seen for **SEO[1-1]-Li** and the largest for **SEO[1-10]-Li**. When comparing values of χ, significant discrepancies were observed in samples as they deviated from symmetric volume fractions. As previously mentioned, Balsara and coworkers developed eqn 1 from SEO diblocks at or near symmetric volume fractions; consequently, a deviation is not surprising. However, χ_{RPA} seemed to deviate from χ_{eff} similarly when moving to the left or right of $f_{PEO} = 0.5$ (where f_{PEO} is volume fraction of PEO swollen with salt for all samples with the –Li suffix). For example, when $f_{PEO} = 0.24$ and 0.78 (samples **SEO[4-1]** and **SEO[1-4]**, respectively), there is a roughly 55% increase for χ_{RPA} compared with χ_{eff}. Likewise, when $f_{PEO} = 0.11$ and 0.91 (samples **SEO[10-1]** and **SEO[1-10]**, respectively) an increase of nearly 350% for both samples was observed for χ_{RPA}. Because of the apparent symmetric dependence of χ_{RPA} on f_{PEO}, a straightforward volume fraction dependent correction to the Balsara χ prediction equation can be made, such that the equation remains unchanged at $f_{PEO} = 0.5$ but increases appropriately at asymmetric volume fractions. Unfortunately, as only one salt concentration was assessed ($r = 0.1$), this modification is likely only valid at this salt ratio. The percent increase in χ can be fit to the form of

$$\%\ increase = \alpha e^{\beta(f_{PEO}-\gamma)^2} + \varepsilon \qquad (2)$$

By multiplying the original χ_{eff} equation by the expression previously, our MBC thermodynamic data are corrected. Constants α, β, γ, and ε can be found in the SI.

A possible explanation of this large increase in χ_{RPA} at asymmetric volume fractions may have to do with the inability of PS to mix and disturb the lithium bound PEO structure. Thus, even at very low volume fractions, phase separation without long range order persists. In fact, the $(\chi N)_{RPA}$ for **SEO[10-1]-Li** and **SEO[1-10]-Li** is 79 and 57, respectively, suggesting both samples fit in the sphere morphology regime for both the mean-field diblock phase diagram as well as Matsen's MBC phase diagram prediction.[19] Therefore, it may be that perhaps these samples thermodynamically prefer the sphere state but remain disordered because of the kinetic trapping of the multiblock architecture. It is also worth noting that the norbornene linker was omitted while fitting, which could have an effect on the resulting

Table 2. R_g and χ values as determined by the random phase approximation fit, as well as predicted χ

MBC	R_g (nm)	χ_{eff}	χ_{RPA}	% Difference	N	f_{PEO}[a]
SEO[10-1]-Li	3.8	0.11	0.48	+330	120	0.11
SEO[4-1]-Li	2.6	0.19	0.29	+57	61	0.24
SEO[1-1]-Li	1.8	0.30	0.27	−12	34	0.51
SEO[1-4]-Li	3.8	0.14	0.21	+52	89	0.78
SEO[1-10]-Li	7.1	0.072	0.33	+360	240	0.91

MBC, multiblock copolymer; PEO, polyethylene oxide.
[a]Volume fraction of PEO swollen with lithium *bis*-(trifluoromethane)sulfonimide salt.

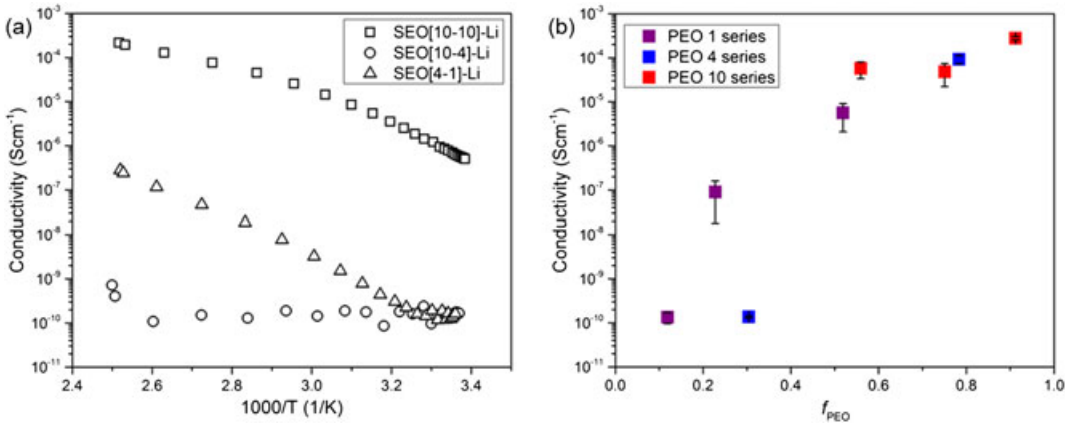

Figure 8. (a) Representative electrochemical impedance spectroscopy data for highly conductive [**SEO(10-10)-Li**, squares], moderately conducting [**SEO**(**4-1**)-Li, triangles], and poorly conducting [**SEO**(**10-4**)-**Li**, circles] samples. (b) Triplicate data for conductivity at 80 °C. Samples are color-coded based on polyethylene oxide (PEO) macromonomer, **PEO 1** (purple), **PEO 2** (blue), and **PEO 3** (red). PEO volume fraction (f_{PEO}) represent PEO volume fraction swollen with salt. This figure is available in colour online at wileyonlinelibrary.com/journal/pat

values. However, based on the molar mass and stoichiometry of the norbornene units, the contribution of these linkers to the overall MBC should be minimal.

Electrochemical impedance spectroscopy

Samples with LiTFSI were tested for lithium ion conductivity using EIS. Triplicate data of conductivity are shown at 80 °C, as well as three representative Arrhenius plots of ion conductivity (Fig. 8). In general, samples with lower volume fractions of PEO had low conductivity, with the exception of **SEO[4-1]-Li**, which displayed moderate conductivity even compared with some samples with higher PEO volume fractions. As determined by SAXS, **SEO[4-1]** should be in the disordered state, which, compared with a morphology in which PEO would not percolate, would have substantially higher conductivity.[43,52] A threshold volume fraction seems to exist near $f_{PEO} = 0.5$, below which samples show effectively no conductivity, and above which samples conduct similarly. This is noteworthy, as **SEO[10-10]-Li** contained a substantial amount of PS ($f_{PS} = 0.44$), but had a conductivity comparable with if not higher than **SEO[4-10]-Li** and **SEO[1-10]-Li**. We believe that the MBC architecture increases the number of grain boundaries, or at least makes phases with conductive paths in numerous orientations, as seen in the electron micrograph of **SEO[10-10]**. As Balsara and coworkers have recently shown, increasing the number of defects increases overall ion conductivity.[37]

CONCLUSION

A molecular weight series of PS–PEO MBCs was synthesized using the thiol–norbornene reaction, by combining telechelic di-thiol and di-norbornene macromonomers. The resulting materials were studied neat by WAXS, DSC, SAXS, and TEM. Crystallinity within samples trended with increasing PEO content and induced phase separation as determined by SAXS. Disordered microphase separation was seen in **SEO[10-10]** via TEM, and a SAXS peak persisted even at higher temperatures, above the melting point of PEO. The observed phase separation for **SEO [10-10]** is likely formed during annealing and thus not an artifact of crystallinity.

Lithium *bis*-(trifluoromethane)sulfonimide was dissolved [(Li)/(EO) = 0.1] in the MBCs to analyze their properties as BCEs, as well as assessed them for lithium ion conduction. All samples demonstrated some degree of phase separation at room temperature, no longer driven by crystallinity, as determined by SAXS and DSC. Four of the nine samples had broad higher ordered peaks via SAXS, indicating that indeed a specific morphology was present, but that microphase ordering was not consistent. The other five samples had disordered scattering peaks, which were analyzed using the RPA fit. The resulting χ values were compared to a recent prediction specific for symmetric SEO diblock copolymers. A good fit was found for a sample with f_{PEO} near 0.5. Asymmetric samples deviated greatly from the prediction, with significantly larger χ values that seemed to diverge symmetrically on either side of $f_{PEO} = 0.5$; a modification to the reported equation was introduced that corrected χ with respect to volume fraction.

Salty samples were also assessed for lithium ion conductivity using EIS. Samples with f_{PEO} at or above 0.5 demonstrated high and nearly uniform lithium ion conductivity, whereas samples in the succeeding text had little to no conductivity. An exception was **SEO[4-1]-Li**, which, regardless of its low f_{PEO} (0.24), demonstrated moderate conductivity. The ease of synthesis of these samples, their encouraging conductivities, and their interesting properties observed here by SAXS, TEM, and RPA fitting, underscore the importance of continued research into multiblock copolymers, both fundamental and applied. We plan on continuing our investigations of these materials as potential lithium ion battery separators.

CONFLICT OF INTEREST

The authors declare no competing financial interest.

AUTHOR CONTRIBUTIONS

The manuscript was written through contributions of all authors. All authors have given approval to the final version of the manuscript.

Acknowledgements

This work was funded by the Office of Naval Research (N00014-10-1-0348), NSF-EAPSI award number IIA-1414768, and the JSPS Summer Program. The authors would like to thank Prof. R. Hayward and R. Selhorst for thoughtful scientific discussion, as well as C. Backlund and K. McLeod for assisting with manuscript preparation. We also thank R. Adhikari and Prof. M. Touminen for maintaining the EIS instrument.

REFERENCES

[1] M. Matsen, M. Schick, *Phys. Rev. Lett.* **1994**, *72*, 2660–2663.
[2] M. W. Matsen, F. S. Bates, *Macromolecules* **1996**, *29*, 7641–7644.
[3] M. W. Matsen, F. S. Bates, *Macromolecules* **1996**, *29*, 1091–1098.
[4] F. Bates, *Annu. Rev. Phys. Chem.* **1990**, *41*, 525–557.
[5] J. Bang, S. H. Kim, E. Drockenmuller, M. J. Misner, T. P. Russell, C. J. Hawker, *J. Am. Chem. Soc.* **2006**, *128*, 7622–7629.
[6] C. Park, J. Yoon, E. L. Thomas, *Polymer* **2003**, *44*, 6725–6760.
[7] G. Riess, *Prog. Polym. Sci.* **2003**, *28*, 1107–1170.
[8] K. Kataoka, A. Harada, Y. Nagasaki, *Adv. Drug Deliv. Rev.* **2001**, *47*, 113–131.
[9] E. S. Gil, S. M. Hudson, *Prog. Polym. Sci.* **2004**, *29*, 1173–1222.
[10] M. Behl, A. Lendlein, *Mater. Today* **2007**, *10*, 20–28.
[11] J. J. Huang, H. Keskkula, D. R. Paul, *Polymer* **2004**, *45*, 4203–4215.
[12] P. D. Topham, A. J. Parnell, R. C. J. Hiorns, *Polym. Sci. Part B Polym. Phys.* **2011**, *49*, 1131–1156.
[13] F. S. Bates, *Science* **1991**, *251*, 898–905.
[14] D. A. Hajduk, P. E. Harper, S. M. Gruner, C. C. Honeker, G. Kim, E. L. Thomas, L. J. Fetters, *Macromolecules.* **1994**, *27*, 4063–4075.
[15] H. Hasegawa, H. Tanaka, K. Yamasaki, T. Hashimoto, *Macromolecules* **1987**, *20*, 1651–1662.
[16] F. S. Bates, M. A. Hillmyer, T. P. Lodge, C. M. Bates, K. T. Delaney, G. H. Fredrickson, *Science* **2012**, *336*, 434–440.
[17] L. Wu, E. W. Cochran, T. P. Lodge, F. S. Bates, *Macromolecules* **2004**, *37*, 3360–3368.
[18] M. W. Matsen, M. Schick, *Macromolecules* **1994**, *27*, 7157–7163.
[19] M. W. Matsen, *Macromolecules* **2012**, *45*, 2161–2165.
[20] I. Lee, T. R. Panthani, F. S. Bates, *Macromolecules* **2013**, *46*, 7387–7398.
[21] A. Phatak, L. S. Lim, C. K. Reaves, F. S. Bates, *Macromolecules* **2006**, *39*, 6221–6228.
[22] C. M. Koo, M. A. Hillmyer, F. S. Bates, *Macromolecules* **2006**, *39*, 667–677.
[23] I. Lee, F. S. Bates, *Macromolecules* **2013**, *46*, 4529–4539.
[24] P. L. Golas, K. Matyjaszewski, *Chem. Soc. Rev.* **2010**, *39*, 1338–1354.
[25] G. Gody, T. Maschmeyer, P. B. Zetterlund, S. Perrier, *Nat. Commun.* **2013**, *4*, 2505.
[26] O. Jeon, S. H. Lee, S. H. Kim, Y. M. Lee, Y. H. Kim, *Macromolecules* **2003**, *36*, 5585–5592.
[27] W. Wang, T. Li, T. Yu, F. Zhu, *Macromolecules* **2008**, *41*, 9750–9754.
[28] K. Luo, J. Yang, P. Kopečková, J. Kopeček, *Macromolecules* **2011**, *44*, 2481–2488.
[29] H. Pan, J. Yang, P. Kopečková, J. Kopeček, *Biomacromolecules* **2011**, *12*, 247–252.
[30] C. N. Walker, J. M. Sarapas, V. Kung, A. L. Hall, G. N. Tew, *ACS Macro Lett.* **2014**, *3*, 453–457.
[31] S. P. S. Koo, M. M. Stamenović, R. A. Prasath, A. J. Inglis, F. E. Du Prez, C. Barner-Kowollik, W. Van Camp, T. J. Junkers, *Polym. Sci. Part A Polym. Chem.* **2010**, *48*, 1699–1713.
[32] C. E. Hoyle, T. Y. Lee, T. J. Roper, *Polym. Sci. Part A Polym. Chem.* **2004**, *42*, 5301–5338.
[33] B. H. Northrop, R. N. J. Coffey, *Am. Chem. Soc.* **2012**, *134*, 13804–1213817.
[34] P. Derboven, D. R. D'Hooge, M. M. Stamenovic, P. Espeel, G. B. Marin, F. E. Du Prez, M. F. Reyniers, *Macromolecules* **2013**, *46*, 1732–1742.
[35] W. Young, J. N. L. Albert, A. B. Schantz, T. H. Epps, *Macromolecules* **2011**, *44*, 8116–8123.
[36] I. Nakamura, Z.-G. Wang, *Soft Matter* **2012**, *8*, 9356–9367.
[37] M. Chintapalli, X. C. Chen, J. L. Thelen, A. A. Teran, X. Wang, B. A. Garetz, N. P. Balsara, *Macromolecules* **2014**, *47*, 5424–5431.
[38] D. T. Hallinan, N. P. Balsara, *Annu. Rev. Mater. Res.* **2013**, *43*, 503–525.
[39] M. W. Schulze, L. D. McIntosh, M. A. Hillmyer, T. P. Lodge, *Nano Lett.* **2014**, *14*, 122–126.
[40] C. N. Walker, K. C. Bryson, R. C. Hayward, G. N. Tew, *ACS Nano* **2014**, *8*, 12376–12385.
[41] W. S. Young, T. H. Epps, *Macromolecules* **2009**, *42*, 2672–2678.
[42] A. Panday, S. Mullin, E. D. Gomez, N. Wanakule, V. L. Chen, A. Hexemer, J. Pople, N. P. Balsara, *Macromolecules* **2009**, *42*, 4632–4637.
[43] N. S. Wanakule, A. Panday, S. A. Mullin, E. Gann, A. Hexemer, N. P. Balsara, *Macromolecules* **2009**, *42*, 5642–5651.
[44] X. Wang, J. L. Thelen, A. A. Teran, M. Chintapalli, I. Nakamura, Z.-G. Wang, M. C. Newstein, N. P. Balsara, B. A. Garetz, *Macromolecules* **2014**, *47*, 5784–5792.
[45] A. A. Teran, N. P. J. Balsara, *Phys. Chem. B* **2014**, *118*, 4–17.
[46] L. Leibler, *Macromolecules* **1980**, *13*, 1602–1617.
[47] J. Cui, M. A. Lackey, A. E. Madkour, E. M. Saffer, D. M. Griffin, S. R. Bhatia, A. J. Crosby, G. N. Tew, *Biomacromolecules* **2012**, *13*, 584–588.
[48] C. N. Walker, C. Versek, M. Touminen, G. N. Tew, *ACS Macro Lett.* **2012**, *1*, 737–741.
[49] T. G. Fox, P. J. J. Flory, *Appl. Phys.* **1950**, *21*, 581–591.
[50] J. M. Tarascon, M. Armand, *Nature* **2001**, *414*, 359–367.
[51] I. W. Hamley, V. Castelletto, *Prog. Polym. Sci.* **2004**, *29*, 909–948.
[52] A. A. Teran, S. A. Mullin, D. T. Hallinan, N. P. Balsara, *ACS Macro Lett.* **2012**, *1*, 305–309.

SUPPORTING INFORMATION

Supporting information may be found in the online version of this article.